

MPI-PhT/2002-62
hep-ph/0210380

Associated Higgs production with heavy quark pairs at hadron colliders[†]

STEFAN DITTMAIER

*Max-Planck-Institut für Physik (Werner-Heisenberg-Institut)
Föhringer Ring 6, D-80805 München, Germany*

Abstract

The reactions $p\bar{p}/pp \rightarrow t\bar{t}H + X$ represent important channels in the search for the Standard Model Higgs boson at the Tevatron and the LHC. In the leading perturbative order the cross sections suffer from severe (renormalization and factorization) scale uncertainties. The next-to-leading order QCD corrections stabilize the cross sections considerably. The calculation of these corrections is briefly reviewed, and a few numerical results are discussed.

October 2002

[†]To appear in the proceedings of *The 10th International Conference on Supersymmetry and Unification of Fundamental Interactions, SUSY02*, June 2002, DESY Hamburg

Associated Higgs production with heavy quark pairs at hadron colliders

STEFAN DITTMAIER

*Max-Planck-Institut für Physik (Werner-Heisenberg-Institut)
Föhringer Ring 6, D-80805 München, Germany*

Abstract

The reactions $p\bar{p}/pp \rightarrow t\bar{t}H + X$ represent important channels in the search for the Standard Model Higgs boson at the Tevatron and the LHC. In the leading perturbative order the cross sections suffer from severe (renormalization and factorization) scale uncertainties. The next-to-leading order QCD corrections stabilize the cross sections considerably. The calculation of these corrections is briefly reviewed, and a few numerical results are discussed.

1 Introduction

One of the most pressing open questions in high-energy physics concerns the mechanism of electroweak symmetry breaking. In the electroweak Standard Model (SM) and its extensions, the symmetry breaking is realized spontaneously by the Higgs mechanism which predicts the existence of Higgs bosons. Thus, the search for Higgs bosons is among the first incentives in present high-energy experiments. For the SM Higgs boson, a lower experimental mass limit of $M_H > 114.4$ GeV (95% C.L.) has been set by the LEP experiments [1]. Moreover, an upper bound of $M_H < 196$ GeV (95% C.L.) [2] results from a fit of the SM parameters in the predictions for electroweak precision data.

In the near future, the search for Higgs bosons will continue at the $p\bar{p}$ collider Tevatron [3] and later at the pp collider LHC [4]. Among the various discovery channels for Higgs bosons in the intermediate mass range, Higgs-boson radiation off top quarks, $p\bar{p}/pp \rightarrow t\bar{t}H + X$, plays an important rôle. Although the expected rate is low at the Tevatron, a sample of a few but very clean events could be observed for $M_H \lesssim 140$ GeV [5]. At the LHC, $t\bar{t}H$ production is an important search channel for $M_H \lesssim 125$ GeV [6]. Moreover, analyzing the $t\bar{t}H$ production rate at the LHC can provide valuable information on the top-Higgs Yukawa coupling [7].

Pure leading-order (LO) predictions for the $p\bar{p}/pp \rightarrow t\bar{t}H + X$ cross sections, which have been available in the literature [8] for a long time, are notoriously imprecise, since

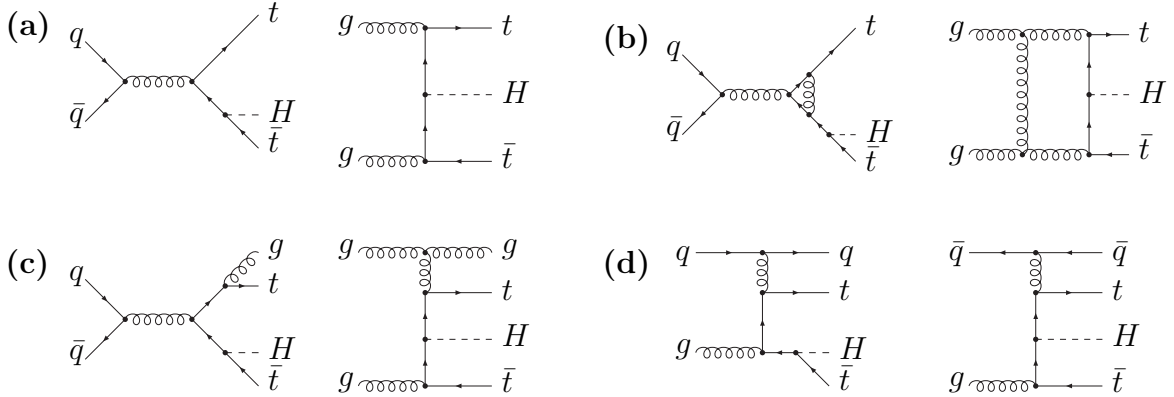


Figure 1: A generic set of diagrams (a) for the Born level, (b) one-loop corrections, (c) gluon radiation and (d) parton splitting in the subprocesses $q\bar{q}, gg \rightarrow t\bar{t}H$ etc.

they suffer from considerable uncertainties owing to the strong dependence on the renormalization and factorization scales. This uncertainty can only be reduced by including higher-order QCD corrections. More recently the complete calculation of the next-to-leading order (NLO) QCD corrections to the total cross section at the Tevatron as well as the LHC was presented in Ref. [9]. These results are in agreement with the parallel calculation of Ref. [10] where, however, only the $q\bar{q}$ annihilation subprocess, which dominates at the Tevatron, has been taken into account. As expected, in the NLO predictions of the cross sections the scale dependence is reduced significantly.

In this brief article the salient features of the calculation [9, 11] of the full NLO QCD corrections are summarized. In the next section, the main obstacles in the actual calculation and the basic ideas of their solution are explained; a detailed description with explicit results is contained in Ref. [11]. Finally, a few examples for phenomenological results are discussed, including the scale dependence of the total cross sections at the Tevatron and the LHC as well as the transverse-momentum and rapidity distributions of the Higgs boson at the Tevatron; more detailed results can be found in Refs. [9, 11].

2 Features of the NLO calculation

(i) General remarks

A survey of typical Feynman diagrams contributing to the processes $p\bar{p}/pp \rightarrow t\bar{t}H + X$ in LO and NLO is shown in Fig. 1. In LO the hadron collisions proceed via $q\bar{q}$ annihilation and gg scattering at the parton level, as illustrated in Fig. 1(a). In NLO, virtual corrections are induced by one-loop diagrams, such as depicted in Fig. 1(b), and real corrections are induced by gluon bremsstrahlung and by parton splittings $q \rightarrow qg$, $\bar{q} \rightarrow \bar{q}g$ in the initial state, as shown in Figs. 1(c) and (d), respectively. Among the one-loop diagrams, the pentagons, which have five internal propagators in the loop, are most complicated. The idea of the analytical calculation and the strategy for a numerically stable evaluation of these pentagons are sketched in the next subsection. The most complicated part in the real corrections concerns the extraction of the infrared (IR) singularities and their proper cancellation; this is briefly described at the end of this section.

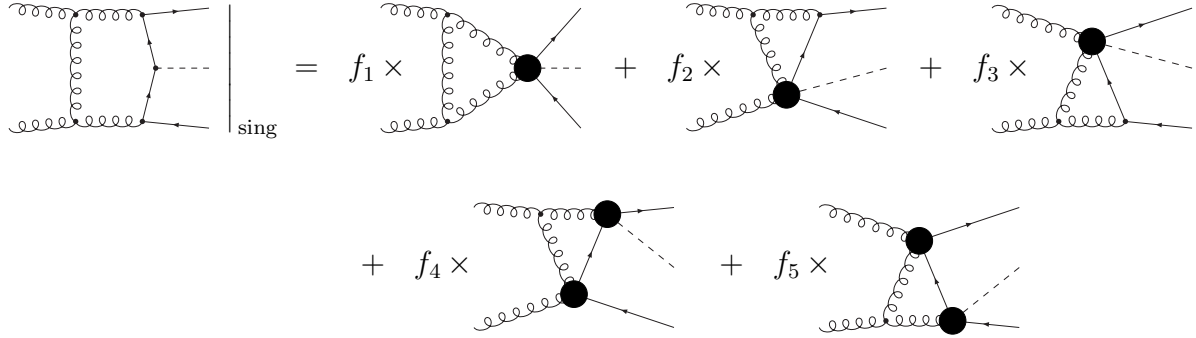


Figure 2: Diagrammatical decomposition of the singular part of a pentagon diagram in terms of triangle diagrams, where the blobs result from shrinking propagators to a point and the f_i denote simple kinematical prefactors.

(ii) Virtual corrections and pentagon diagrams

The main complications in the calculation of the pentagon diagrams are IR (soft and collinear) singularities. The most convenient way to regularize these divergences is dimensional regularization. As known for a long time [12], in $D = 4$ dimensions all 5-point functions can be expressed in terms of 4-point functions, simplifying the calculation considerably. In order to derive a similar reduction of 5-point functions to related 4-point functions in D dimensions, first the dimensionally regularized integral $E^{(D)}$ is translated into another regularization scheme that is defined for $D = 4$. For instance, it is possible to endow all massless propagators in the loop with an infinitesimal mass λ , defining the new integral $E^{(\text{mass},D)}$, which is identical to $E^{(D)}$ if $\lambda = 0$. In the next step, a related *well-defined* integral, denoted $E_{\text{sing}}^{(\text{mass},D)}$, is determined that possesses the same IR singularity structure as $E^{(\text{mass},D)}$. This integral is obtained by decomposing the integrand of the 5-point function in the collinear/soft limit in terms of 3-point integrands with regularization-scheme-independent kinematical prefactors. The explicit construction of $E_{\text{sing}}^{(\text{mass},D)}$ is described in Ref. [11] in detail and illustrated in Fig. 2 for a specific example diagrammatically. The difference of the two integrals, $E^{(\text{mass},D)} - E_{\text{sing}}^{(\text{mass},D)}$, has a uniquely-determined integrand and it is regularization-scheme independent, i.e. the limits $D \rightarrow 4$ and $\lambda \rightarrow 0$ commute in this quantity. In total, we have generated in this way the relation

$$E^{(D)} - E_{\text{sing}}^{(D)} + \mathcal{O}(D-4) = E^{(\text{mass},D=4)} - E_{\text{sing}}^{(\text{mass},D=4)} + \mathcal{O}(\lambda), \quad (2.1)$$

where $\lambda = 0$ on the l.h.s. and $D = 4$ on the r.h.s. Consequently, solving Eq. (2.1) for $E^{(D)}$,

$$E^{(D)} = E_{\text{sing}}^{(D)} + [E^{(\text{mass},D=4)} - E_{\text{sing}}^{(\text{mass},D=4)}] + \dots, \quad (2.2)$$

this integral is expressed (up to irrelevant terms indicated by the ellipsis) in terms of four-dimensional integrals and D -dimensional 3-point functions.

The translation of D -dimensional integrals into four dimensions works not only for complete Feynman diagrams, but also for individual scalar and tensor integrals. As shown in Ref. [12], for $D = 4$ the scalar 5-point function E_0 can be expressed in terms of a linear combination of five 4-point functions. Thus, Eq. (2.2) expresses $E_0^{(D)}$ in terms of scalar 3- and 4-point functions. For the evaluation of 5-point tensor integrals, two entirely different

methods have been used. In one calculation the well-known Passarino–Veltman algorithm [13] is adopted to algebraically reduce the tensor coefficients recursively to tensors of lower rank, eventually leading to scalar integrals. This procedure requires to solve a set of linear equations for each tensor rank and, in this way, adds a factor of an inverse Gram determinant in each step. At the phase-space boundary the Gram determinants vanish, since the momenta that span the tensors become linearly dependent. Near the phase-space boundary this leads to numerical instabilities that are controlled by careful extrapolation out of the safe inner phase-space domains. The second calculation, however, avoids the appearance of leading Gram determinants (i.e. Gram determinants formed by four momenta) by using the method of Ref. [14], which is based on a generalization of the strategy [12] for scalar 5-point functions and reduces 5-point tensor coefficients to 4-point integrals directly. Applying this alternative renders the virtual correction near the phase-space boundary much more stable than in the usual Passarino–Veltman approach, and the extrapolation from the inner part of phase space turns out to be practically unnecessary. The results obtained by the two methods mutually agree with each other.

(iii) Real corrections and IR singularities

Although the $2 \rightarrow 4$ scattering matrix element of the real NLO correction σ^{real} [see Figs. 1(c) and (d)] are quite involved, they still could be calculated by conventional trace techniques or by using the MADGRAPH package [15]. The IR (soft and collinear) singularities appearing in the phase-space integral of the squared matrix elements have to be treated in dimensional regularization and they must be extracted before the numerical integration over the four-particle phase space. To this end, a generalization [16] of the dipole subtraction formalism [17] to massive quarks has been adopted. In this formalism the singularities of the cross section σ^{real} are mapped onto a suitably chosen auxiliary cross section σ^{sub} so that the difference $\sigma^{\text{real}} - \sigma^{\text{sub}}$ can safely be integrated numerically in four dimensions. Moreover, σ^{sub} is still simple enough to allow for an analytical integration over the singular regions in phase space. The result of this integration consists of LO cross sections dressed by universal functions that contain the singularities. This integrated cross section is decomposed into a part $\bar{\sigma}_1^{\text{sub}}$ that, defined on configurations with LO kinematics, cancels the soft and collinear singularities of the virtual corrections; and a second part $\bar{\sigma}_2^{\text{sub}}$ that includes the singularities from initial-state parton splitting, which are absorbed in the renormalization of the parton densities. Thus the total NLO correction $\Delta\sigma^{\text{NLO}}$ can be written as the sum

$$\Delta\sigma^{\text{NLO}} = [\sigma^{\text{real}} - \sigma^{\text{sub}}] + [\sigma^{\text{virtual}} + \bar{\sigma}_1^{\text{sub}}] + [\sigma^{\text{part}} + \bar{\sigma}_2^{\text{sub}}], \quad (2.3)$$

in which each bracket is separately finite.

3 Some numerical results

Figure 3 shows the total cross sections for $t\bar{t}H$ production at the Tevatron and the LHC for a fixed Higgs-boson mass of $M_H = 120$ GeV as function of the renormalization and factorization scales, which have been taken at the common value μ . It has been checked that no accidental compensations of scale dependences are introduced by this

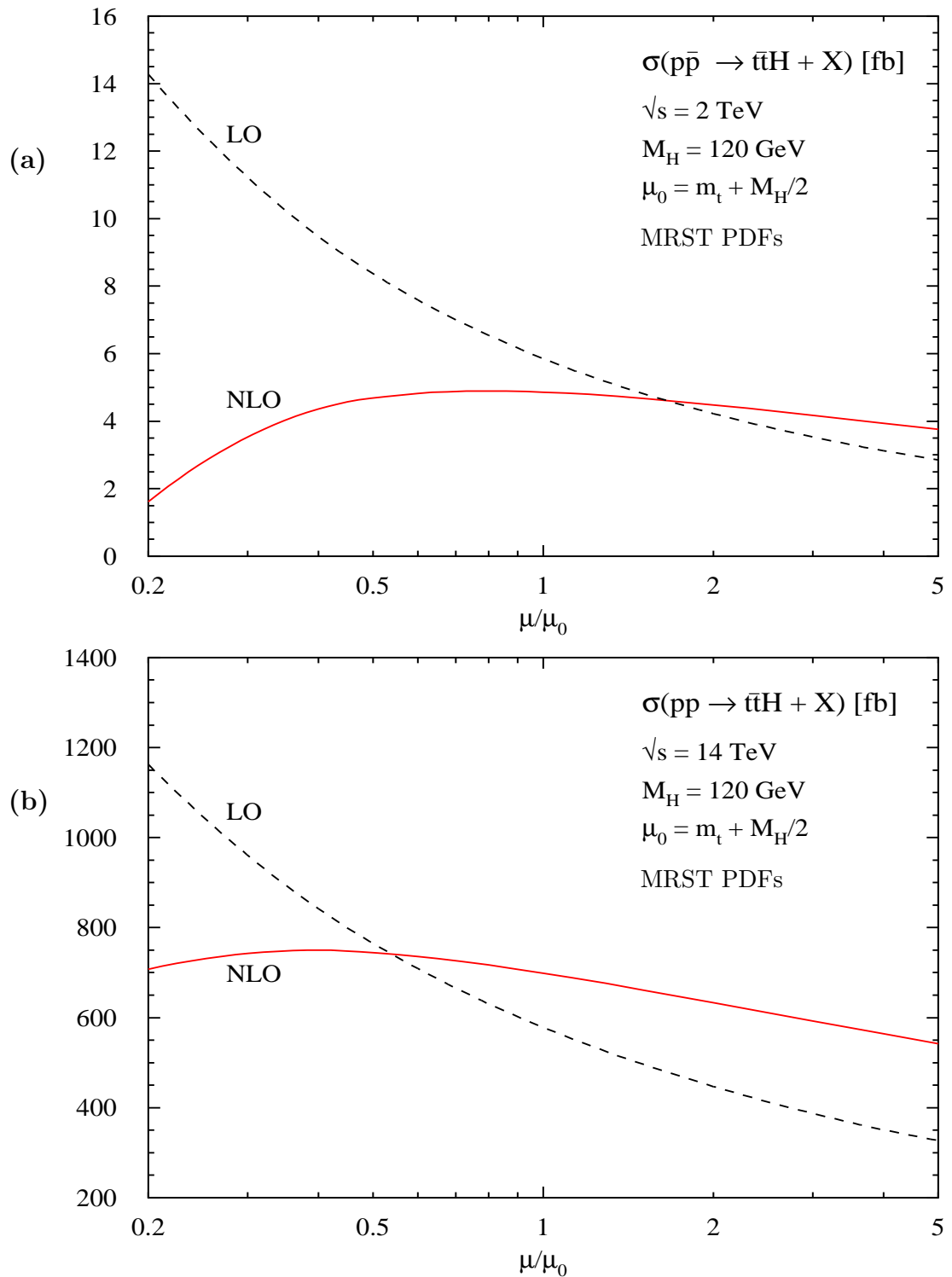


Figure 3: Variation of the LO and NLO cross sections with the renormalization and factorization scales for (a) $p\bar{p} \rightarrow t\bar{t}H + X$ at Tevatron and (b) $pp \rightarrow t\bar{t}H + X$ at the LHC.

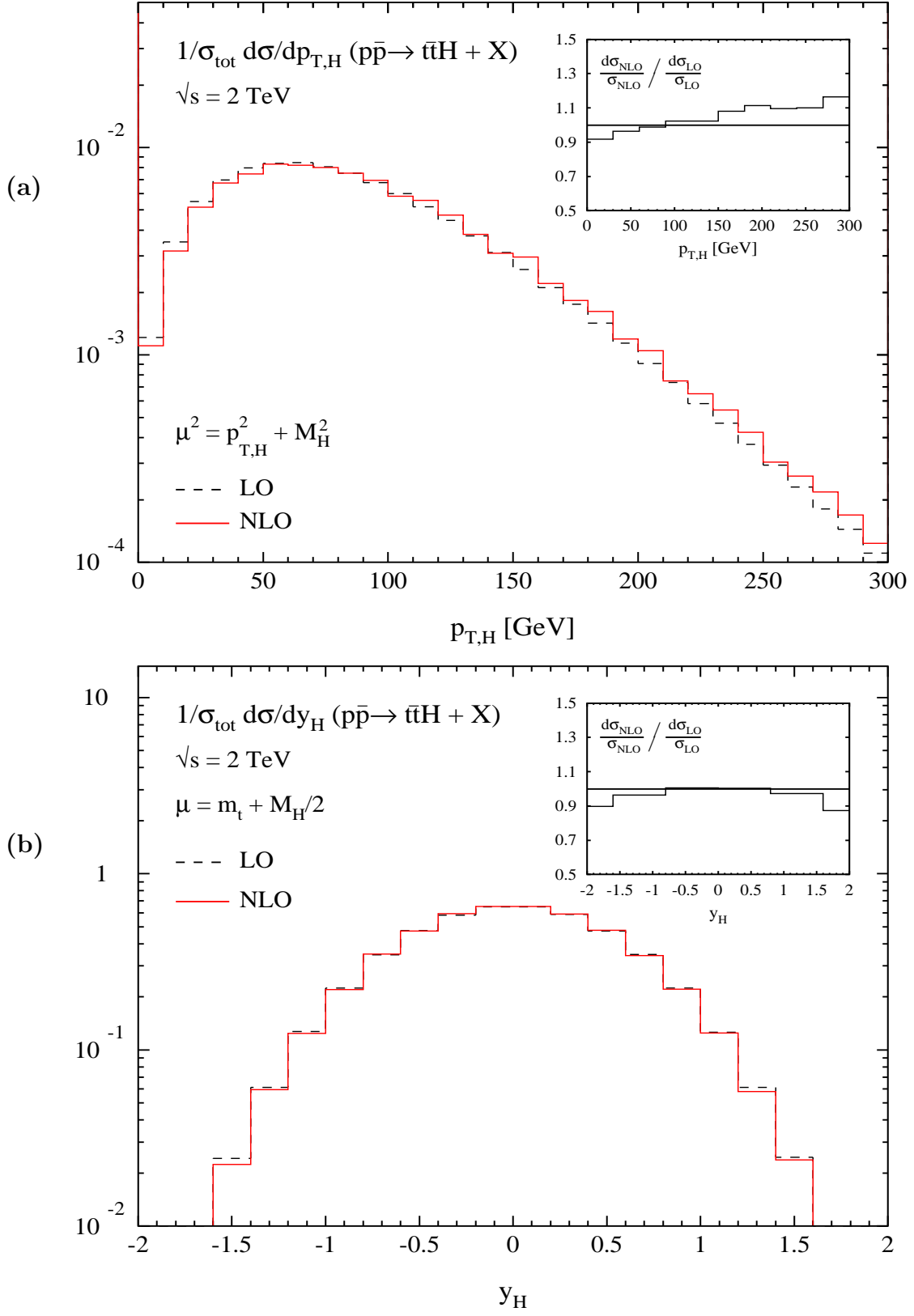


Figure 4: (a) Normalized transverse-momentum distribution and (b) rapidity distribution of the Higgs boson in LO and NLO for $p\bar{p} \rightarrow t\bar{t}H + X$ at the Tevatron ($M_H = 120$ GeV).

identification. In the vicinity of the central scale $\mu_0 = (2m_t + M_H)/2$, the NLO cross sections are remarkably stable with very little variation for μ between $\sim \mu_0/3$ and $\sim 3\mu_0$, in contrast to the LO approximation for which the production cross section changes by more than a factor 2 within the same interval. The relative corrections, which are quantified by K factors, $K = \sigma_{\text{NLO}}/\sigma_{\text{LO}}$ (with all quantities calculated consistently in NLO and LO, respectively) are nearly constant in the Higgs-boson mass range $M_H = 100\text{--}250\text{ GeV}$.

Although at the Tevatron the cross section is strongly dominated by $q\bar{q}$ annihilation for scales $\mu \sim \mu_0$, the proper study of the scale dependence requires inclusion of the gg , gq , and $g\bar{q}$ channels. If μ is chosen too low, large logarithmic corrections spoil the convergence of perturbation theory, as indicated by the negative NLO cross section for $\mu \lesssim \mu_0/5$. Apparently the K factor varies from ~ 0.8 at the central scale $\mu = \mu_0$ to ~ 1.0 at the threshold scale $\mu = 2\mu_0$. As explained in Ref. [9], the value of the K factor below unity can be understood intuitively in the fragmentation picture proposed in Ref.[18], although the kinematical limit justifying this approximation is not yet realized at the Tevatron.

At the LHC the major part of the cross section is due to the gg channel, which gives rise to increased gluon radiative corrections. For the central scale μ_0 the relative corrections amount to $K \sim 1.2$, increasing to ~ 1.4 at the threshold value $\mu = 2\mu_0$. Again the fragmentation picture [18] is approximately compatible with the complete NLO prediction.

Finally, as illustrating examples for final-state distributions, Fig. 4 shows the transverse-momentum and rapidity distributions of the Higgs boson for $p\bar{p} \rightarrow t\bar{t}H + X$ at the Tevatron in LO and NLO approximation. Note that for the distribution in the transverse Higgs-boson momentum $p_{\text{T},H}$, the scale μ is not taken constant but defined by $\mu^2 = p_{\text{T},H}^2 + M_H^2$; this choice is more natural for large transverse momenta. The ratio of the (normalized) NLO and LO distributions reveals that the mere rescaling of the LO distribution by a constant K factor would reproduce the NLO distribution only within $\pm 10\%$ in the most important ranges. For the $p_{\text{T},H}$ distribution the increase of the ratio $d\sigma_{\text{NLO}}/d\sigma_{\text{LO}}$ with increasing $p_{\text{T},H}$ can be traced back to the scale variations of $d\sigma_{\text{NLO}}$ and $d\sigma_{\text{LO}}$, since μ rises with increasing $p_{\text{T},H}$ and $d\sigma_{\text{LO}}$ decreases with increasing μ faster than $d\sigma_{\text{NLO}}$. The respective distributions at the LHC, which are displayed in Ref. [11], show the same qualitative behaviour, but in the $p_{\text{T},H}$ distribution the ratio $d\sigma_{\text{NLO}}/d\sigma_{\text{LO}}$ varies even more strongly with $p_{\text{T},H}$.

4 Conclusion

The strong scale dependence of the LO cross sections for $p\bar{p}/pp \rightarrow t\bar{t}H + X$ is drastically reduced by the NLO calculation, and the theoretical predictions are stabilized. Thus, the NLO cross sections can serve as a solid base for experimental analyses at the Tevatron and the LHC. This improvement is also observed for the final-state Higgs transverse-momentum and rapidity distributions.

References

- [1] The LEP Working Group for Higgs Boson Searches, LHWG Note/2002-01.
- [2] D. Abbaneo *et al.*, hep-ex/0112021.
- [3] M. Carena *et al.*, hep-ph/0010338.
- [4] ATLAS Collaboration, Technical Design Report, Vols. 1 and 2, CERN–LHCC–99–14 and CERN–LHCC–99–15;
CMS Collaboration, Technical Proposal, CERN–LHCC–94–38.
- [5] J. Goldstein, C. S. Hill, J. Incandela, S. Parke, D. Rainwater and D. Stuart, Phys. Rev. Lett. **86** (2001) 1694 [hep-ph/0006311].
- [6] V. Drollinger, T. Müller and D. Denegri, hep-ph/0111312.
- [7] F. Maltoni, D. Rainwater and S. Willenbrock, Phys. Rev. D **66** (2002) 034022 [hep-ph/0202205].
- [8] Z. Kunszt, Nucl. Phys. B **247** (1984) 339;
W. J. Marciano and F. E. Paige, Phys. Rev. Lett. **66** (1991) 2433;
J. F. Gunion, Phys. Lett. B **261** (1991) 510.
- [9] W. Beenakker, S. Dittmaier, M. Krämer, B. Plümper, M. Spira and P. M. Zerwas, Phys. Rev. Lett. **87** (2001) 201805 [hep-ph/0107081].
- [10] L. Reina and S. Dawson, Phys. Rev. Lett. **87** (2001) 201804 [hep-ph/0107101];
L. Reina, S. Dawson and D. Wackerlo, Phys. Rev. D **65** (2002) 053017 [hep-ph/0109066].
- [11] W. Beenakker, S. Dittmaier, M. Krämer, B. Plümper, M. Spira and P. M. Zerwas, DESY 02-177.
- [12] D. B. Melrose, Nuovo Cim. **40** (1965) 181.
- [13] G. Passarino and M. Veltman, Nucl. Phys. B **160** (1979) 151.
- [14] A. Denner and S. Dittmaier, MPI-PhT/2002-63.
- [15] T. Stelzer and W. F. Long, Comput. Phys. Commun. **81** (1994) 357 [hep-ph/9401258];
H. Murayama, I. Watanabe and K. Hagiwara, KEK-91-11.
- [16] S. Catani, S. Dittmaier, M. H. Seymour and Z. Trócsányi, Nucl. Phys. B **627** (2002) 189 [hep-ph/0201036].
- [17] S. Catani and M. H. Seymour, Phys. Lett. B **378** (1996) 287 [hep-ph/9602277] and
Nucl. Phys. B **485** (1997) 291 [Erratum-ibid. B **510** (1997) 291] [hep-ph/9605323].
- [18] S. Dawson and L. Reina, Phys. Rev. D **57** (1998) 5851 [hep-ph/9712400].